View metadata, citation and similar papers at core.ac.uk
brought to you by CORE
provided by Elsevier - Publisher Connector

Current Biology, Vol. 15, 2075–2085, December 6, 2005, ©2005 Elsevier Ltd All rights reserved. DOI 10.1016/j.cub.2005.10.039

Building Complexity: An In Vitro Study of Cytoplasmic Dynein with In Vivo Implications

Roop Mallik,[4,1] Dmitri Petrov,[4,2] S.A. Lex,[3] S.J. King,[3] and S.P. Gross[1,*]
[1] Department of Developmental and Cell Biology
[2] Department of Physics and Astronomy
University of California, Irvine
Irvine, California 92697
[3] Division of Molecular Biology and Biochemistry
School of Biological Sciences
University of Missouri, Kansas City
Kansas City, Missouri 64110

Summary

Background: Cytoplasmic dynein is the molecular motor responsible for most retrograde microtubule-based vesicular transport. In vitro single-molecule experiments suggest that dynein function is not as robust as that of kinesin-1 or myosin-V because dynein moves only a limited distance (approximately 800 nm) before detaching and can exert a modest (approximately 1 pN) force. However, dynein-driven cargos in vivo move robustly over many microns and exert forces of multiple pN. To determine how to go from limited single-molecule function to robust in vivo transport, we began to build complexity in a controlled manner by using in vitro experiments.
Results: We show that a single cytoplasmic dynein motor frequently transitions into an off-pathway unproductive state that impairs net transport. Addition of a second (and/or third) dynein motor, so that cargos are moved by two (or three) motors rather than one, is sufficient to recover several properties of in vivo motion; such properties include long cargo travels, robust motion, and increased forces. Part of this improvement appears to arise from selective suppression of the unproductive state of dynein rather than from a fundamental change in dynein's mechanochemical cycle.
Conclusions: Multiple dyneins working together suppress shortcomings of a single motor and generate robust motion under in vitro conditions. There appears to be no need for additional cofactors (e.g., dynactin) for this improvement. Because cargos are often driven by multiple dyneins in vivo, our results show that changing the number of dynein motors could allow modulation of dynein function from the mediocre single-dynein limit to robust in vivo-like dynein-driven motion.

Introduction

The kinesin and dynein families of microtubule motors transport numerous cellular cargos. Such transport is vital for the maintenance of cellular structure and function [1, 2]. The motors use energy from ATP hydrolysis to bias protein conformational changes, which result in step-like directed motion along microtubule filaments within the cell. Optical trap-based biophysical measurements of motion driven by a single kinesin-1 [3, 4] or dynein [5, 6] under controlled in vitro conditions have provided insight into the mechanochemical cycle of these motors. The discrete steps of motor motion have been measured and connected to the hydrolysis of a single ATP per step, and models [7, 8] for the cycle of the motor have been proposed to explain experimental data.

The characterization of single motors is an important and necessary first step because it allows the investigation of how the fundamental unit of intracellular transport—the molecular motor—functions. However, in vivo motion can differ significantly from the single-motor function observed in vitro. For example, in the cell dynein-driven cargos frequently move over distances of several microns [9, 10]; in contrast, the average run length of single-dynein-driven motion in vitro is less than a micron [11, 12], and even a bead moved in vitro by a combination of dynein and dynactin moves approximately 1.5 μm [11]. Further, compared to the approximately 1 pN force that single dynein exerts in vitro [5], the force required to stall cargos driven by dynein in vivo can exceed 5 pN [13, 14]. This large force implies that in vivo transport potentially uses multiple dynein motors, in addition to non-motor accessory proteins [10, 15–17]. To better understand how useful and robust in vivo transport could occur, we would therefore like to understand how multiple motors working together alter transport properties from those seen for single motors.

In this work, we investigate how limited function of single dynein motors in vitro is improved when more than one motor is used. We show that, in contrast to the robust function of kinesin-1, single cytoplasmic dyneins go through unproductive intervals where the motor is paused or exhibits back-and-forth motion. However, employing more than one dynein motor on a cargo improves performance so that it is comparable to in vivo motion: Cargos move over distances of many microns, and the unproductive periods are suppressed. These results suggest that the poor qualities of motion seen in single dynein motors are not an artifact of the in vitro conditions of our experiments and that dynein has certain limitations that can be corrected by employing multiple motors. We provide evidence that such improvement comes about not from a change in the mechanochemical cycle of the single motor itself but by suppression of the entry of dynein motors into an off-pathway unproductive state. In this off-pathway state, dynein bound cargo can undergo linear diffusive motion while being bound to the microtubule.

Results

Runs Involving Single Cytoplasmic Dyneins Are Short, with Frequent Pauses, Back-and-Forth Motion, and Slippage under Load

We characterized single-dynein function by measuring the run lengths of polystyrene beads (an artificial cargo) moved by dynein. As in earlier in vitro experiments [5], dynein-coated beads were placed on immobilized

*Correspondence: sgross@uci.edu
[4] These authors contributed equally to the paper.

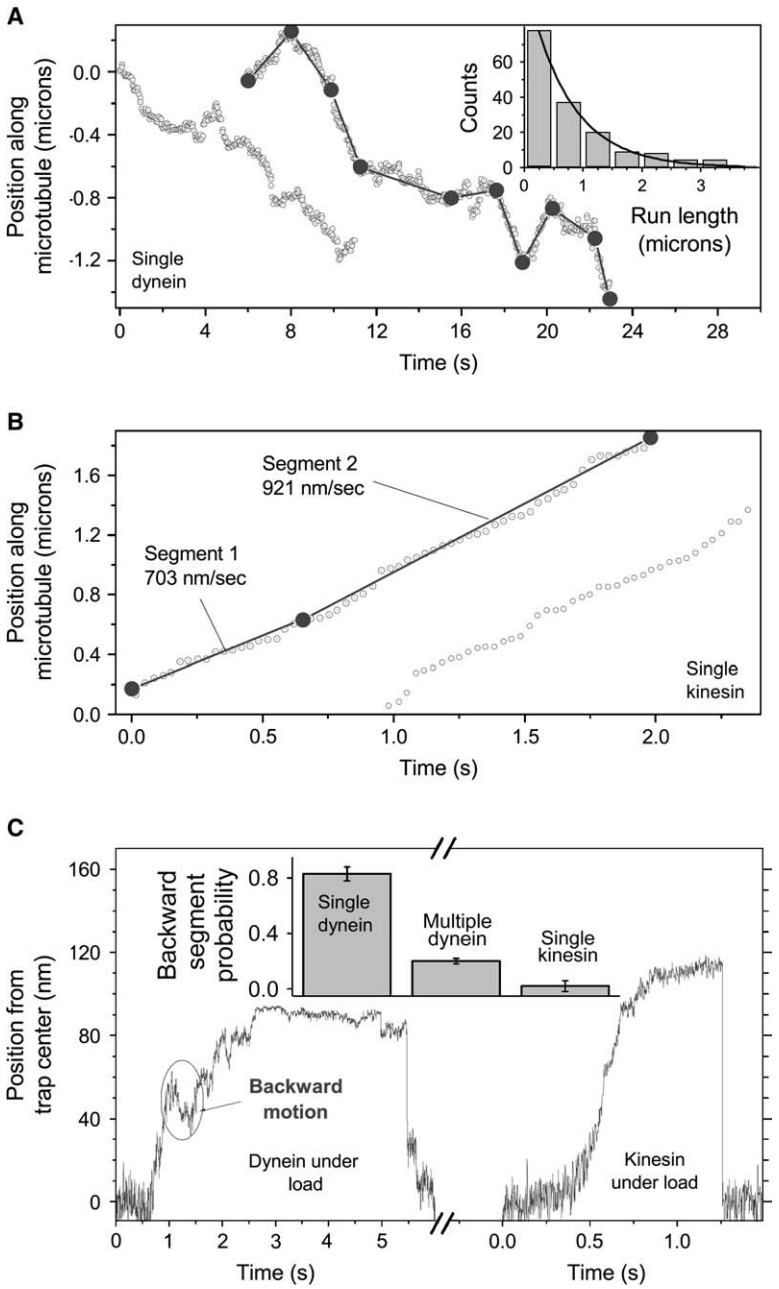

Figure 1. The Single-Dynein Motor Is Not a Robust Transporter

(A) Video tracks of two presumably single-dynein-driven beads moving toward the microtubule minus end. Video tracks end where the bead detached from the microtubule and diffused away. ATP concentration = 2 mM. Note segments of backward motion (motion toward plus end) within the track. Constant-velocity segments generated by the parsing program (see text) are shown as thick gray lines interconnected by closed dots on one video track. The parsing is coarse enough to ignore noisy fluctuations of the bead (see main text). Inset: Distribution of run lengths of single-dynein-driven beads. In total, 161 beads were observed. The run length was determined from video tracks. A thick dark line shows a fit to a single exponential decay (see text). The mean run length was −738 ± 62 nm.

(B) Video tracks of beads driven by a single kinesin-1. The motion is robust and highly directed, with no evidence of backward segments (compare with [A]). Constant-velocity segments generated within one track by the parsing program are shown. Program parameters were exactly same as those used for dynein.

(C) Effect of load on the motion of single-dynein and -kinesin-1 motors. ATP concentration = 3 mM. A typical stall for each motor is shown. For dynein, the optical-trap stiffness was 0.012 pN/nm. Dynein stalled at 90 nm (flat plateau), which corresponds to 1.1 pN of force. The motor detached after a few seconds of stall, and the bead rapidly fell (at approximately the 5.2 s mark) to the trap center (zero position). Backward motion typical of dynein under load is indicated. The backward sliding motion is slower and can therefore be distinguished from motor detachments. For the kinesin stall, the trap stiffness is 0.041 pN/nm. The motor stalled at approximately 4.9 pN. Note the absence of any backward slide. Inset: Probability of finding a backward segment >10 nm in a stall-force record (see main text). The error bars were calculated with the standard deviation of the proportion, $error = \sqrt{\frac{P(1-P)}{N}}$, where P is the proportion of stalls with backward motion and N was the total number of stalls scored.

microtubules (MT) with an optical trap. At the dynein concentration used for single-motor experiments, the probability of more than one motor driving bead motion was <5%, and hence the conclusions from these experiments reflect single-motor function [4]. Once attached to the MT, beads were released from the trap and allowed to move freely before they released from the MT. The total distance moved by the bead before release was measured with video tracking (30 frames/s; see Experimental Procedures). Figure 1A (inset) shows a histogram of run lengths for such presumably single-dynein-driven beads. A characteristic single-exponential decay was observed; this decay likely reflects a constant probability of detachment per step of the single motor from the MT. The mean run length was −738 nm (minus sign implying motion toward the microtubule minus end), in agreement with earlier published results [11, 12]. This result shows that a single dynein motor has less than a 1% chance of moving for more than 3.5 μm in a run. Using a similar assay, we found the mean run length for kinesin-1 to be +1.8 μm (motion toward microtubule plus end; data not shown), which is in agreement with earlier results [11, 18]. Thus, on average, dynein can move only half the distance of a single kinesin-1 motor. This shortcoming of dynein appears to be corrected by the addition of dynactin [11] to levels where it can in principle approximately match kinesin-1, at least as far as run lengths are concerned.

Figure 1A shows two representative video tracks of single-dynein-driven beads moving without applied load. A close examination shows frequent pauses and segments of reverse motion (motion toward the plus

end). Representative video tracks of beads driven by kinesin-1 motors (Figure 1B) show that the motion here is much "smoother" than that of dynein; backward segments and pauses are exceedingly rare, and the bead shows highly directed motion toward the MT plus end. The magnitude of reverse-directed segments for dynein is too large to be explained by thermal fluctuations (flop) of a bead attached to the cargo end of a dynein tether, with the microtubule binding end fixed to the microtubule. To confirm this, we quantified the video tracks of beads tethered by dynein to a microtubule in the absence of ATP (see section 1 in the Supplemental Data available with this article online). Such tethered beads had less than a 1% chance of moving beyond ±100 nm from the tether point, in contrast to the observation of backward segments of up to approximately 800 nm for dynein-driven beads in the presence of ATP. Bidirectional motion of motor-driven cargo in vivo in the presence of both dynein and kinesin motors is well documented [16, 17]. However, in our experiments, only purified dynein motors drove bead motion, and the possibility of reverse/paused segments arising from competition with kinesin-1 can be excluded.

For further comparison, we looked at the motion of dynein- or kinesin-1-driven beads under load in an optical trap (Figure 1C). The stall force of dynein is approximately 1 pN [5, 14], compared to the much larger values (5–6 pN) for kinesin-1 [4]. To compare appropriately, we normalized by total stall force and scored for events of backward motion in a load interval between 50% and 100% of the stall force (i.e., between 0.5 and 1 pN for single dynein and 3 and 6 pN for kinesin-1). We only scored backward motion >10 nm in length and lasting for more than 200 ms beyond 10 nm to avoid counting random bead flops (see section 2 in the Supplemental Data for justification). We found a much higher chance of finding backward motion in dynein than in kinesin (see Figure 1C inset). Therefore, the effect of load appears to be more severe on dynein. Because single dynein motors often enter a paused/back-and-forth state under no load (see Figure 1A), it is possible that this state manifests as the increased backward slippage under load observed in Figure 1C. This might be expected if the microtubule-motor binding is of a weak electrostatic nature in this state [19–21].

This poor quality of single-dynein functions appears not to arise from artifacts due to the in vitro nature of our experiments, as evidenced by analysis of flop of the bead perpendicular to MT and additional experiments (such as using a dynein light-chain antibody to attach dynein to the beads; see section 3 in the Supplemental Data). Finally, later in this paper we identify additional factors that improve single-dynein function under identical in vitro conditions. The identification of these factors, which are relevant to in vivo dynein function, serves as an internal control to show that the poor motion is an inherent property of single-dynein function.

Quantitative Analysis of Dynein Motion

To understand in a quantitative manner the difference between dynein and kinesin-1-driven motion, we developed software (see section 4 in the Supplemental Data) to parse the video track (position along MT versus time) into segments of constant velocity. An example of the parsing can be seen in Figures 1A and 1B (thick, continuous lines, shown for one track in each case). We parsed multiple video tracks of dynein-driven beads at the single-motor limit to generate histograms of segment lengths (Figure 2A) and segment velocities (Figure 2B). The occurrence of reverse motion for dynein (plus-end directed, velocity > 0) is clearly brought out in the histograms; 19% of the net distance moved by dynein is backward, as calculated from the areas in Figure 2A (also see Table 1). This reverse-directed motion leads to a large spread in segment velocities, as measured by the standard deviation of single-dynein segment velocities (σ = 400 nm/s for the velocity distribution in Figure 2B, also see Table 1). The mean velocity within segments of minus-directed motion is −312 nm/s, and the overall mean velocity (counting both minus- and plus-directed segments) is −213 nm/s. The results from parsing are summarized in Table 1. To compare these characteristics of dynein with kinesin-1-driven motion, we performed an identical analysis of kinesin-1-driven beads (Figures 2C and 2D; see Table 1 for calculated values). In contrast to that for dynein, backward motion for kinesin-1 (defined as minus directed) was rare, at < 1% of the total distance moved. This led to a narrower distribution (σ = 278 nm/s; Figure 2D) of segment velocity when compared to that of single dyneins.

Several criteria could be used to characterize robustness of motion. First, the frequency of unproductive pauses and backward motion would indicate how often the motor stalls, backsteps, or goes into an off-pathway state. Second, the average duration of constant velocity segments indicates for how long uninterrupted periods of motion are sustained. Third, the average velocity of the segments and the distribution of segment velocities indicate how much the motor's function varies. A narrow distribution of segment velocities would indicate a motor that hydrolyzes ATP at a relatively constant rate; such a motor would step with a fixed step size and sustain such behavior over long periods of motion. Periods of reverse/backward motion should lead to a broader velocity distribution. These criteria motivate the analysis and quantification of motor function presented hereafter and, through a comparison of single-dynein versus kinesin-1 performance, show that dynein is a poorer transport system (see Table 1).

Estimation of Motor Number from Stall Force: Increase in Run Length and Large Stall Forces at High Dynein Concentration

In vivo, motor-driven cargos (both minus- and plus-end directed) move smoothly over distances of multiple microns [9, 10, 22, 23]. However, the average run lengths for dynein and kinesin-1 in vitro are found to be −0.74 μm (n = 161 runs) and +1.8 μm (n = 105 runs), respectively. If these motors function in the same manner in vivo, it is hard to see how such long motion would be possible with single motors. To test whether additional motors on a cargo can enhance run lengths, we used a combination of optical trap-based force measurement and subsequent free motion of the bead. This was done at appropriately higher concentrations of dynein motors on the bead (see section 5 in the Supplemental Data). In a typical experiment, a trapped bead was first allowed to generate force in the optical trap for a few seconds (typically

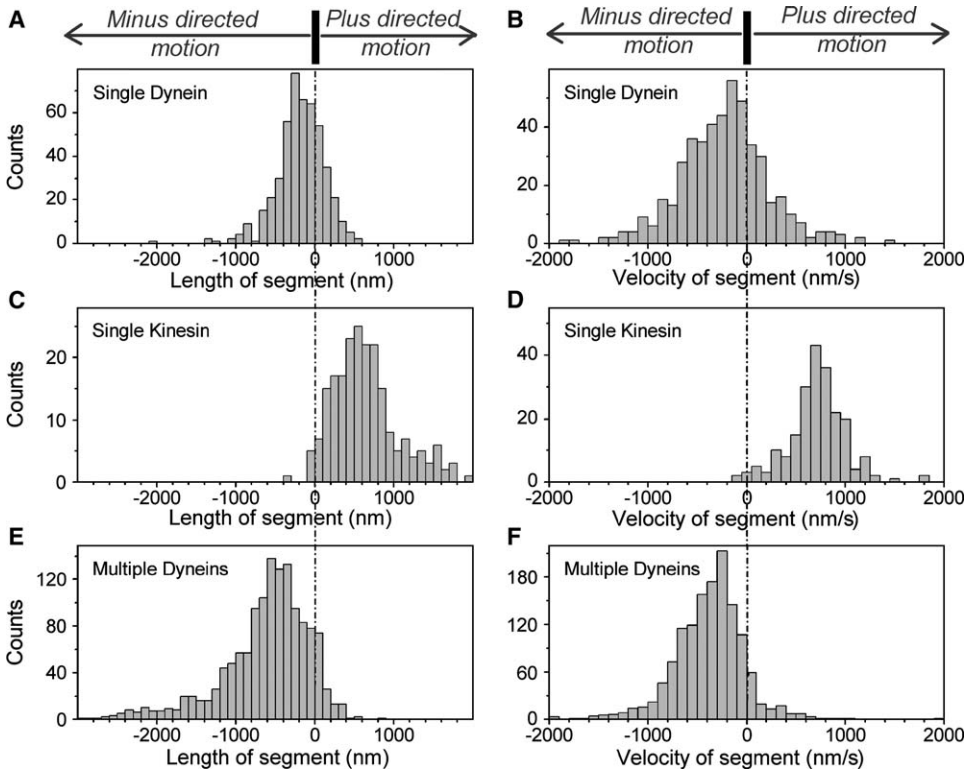

Figure 2. Results of Parsing Dynein and Kinesin-1 Tracks into Constant-Velocity Segments

See Table 1 for values derived from this parsing. Dotted vertical lines divide the plus and minus directions of motion. Net motion is plus directed for kinesin-1 and minus directed for dynein.

(A) Distribution of segment lengths for single-dynein motion. Net motion is toward the minus end, but there is a large population of backward segments.

(B) Distribution of segment velocities for single-dynein motion. Positive velocities correspond to the backward segments.

(C) Distribution of segment lengths for kinesin-1. Backward segments are rare.

(D) Velocity distribution for single-kinesin-1 motors. Note the narrower distribution of velocities (compare to [B]) and the absence of negative-velocity segments.

(E) Distribution of segment lengths for motion driven by two or more dynein motors. There is a reduction of backward segments in comparison to single-dynein motion (compare with [A], also see Table 1). The long tail in minus-end motion signifies that runs were longer on the average and also that velocity states continued uninterrupted.

(F) Segment velocity distribution for multiple-dynein motion. Note the narrower spread in velocity compared to the single-dynein case (compare with [B], also see Table 1). Reduction of backward segments is also reflected in smaller counts on the positive velocity side (compare to [B]).

6–8 stalls) before being released and allowed to move under no-load conditions. Video tracks for the entire process (stalls and free motion) were obtained (see Figure 3). At high dynein concentrations (Figures 3B and 3C), we found that the stall force was usually greater than the single-dynein stall force (approximately 1 pN; Figure 3A), showing that these beads were often driven by two or more motors. In the next section, we show that force exerted by multiple dynein motors is additive (see Figure 4A). Given this additive nature, the above measurement of stall force just prior to free motion allows us to estimate the number of dyneins driving motion of a particular bead (see section 5 in the Supplemental Data). Usually, in vitro experiments investigate function of a single molecular motor at a very dilute concentration of motors on the bead, where the probability of two motors driving motion is negligibly small from Poisson statistics [4, 5, 12, 24], and indeed this is what we did to understand single-dynein function. However, such a probabilistic estimate does not reliably determine the number of active motors on a bead at higher motor concentrations. As demonstrated here, a better estimate can be obtained from stall-force measurements with prior knowledge of the single-motor stall force.

One might argue that additional motors (more than two) could attach to the bead during free motion and thus lead to long runs. We do not believe this is true because subsequent stall-force measurements on moving beads that had previously been stalled at approximately 2 pN (and then released to move) rarely showed stall forces >2 pN. The number of dyneins attached to the bead is not expected to change because all dynein motors were absorbed onto the bead surface and there was no free dynein in the buffer. Typical measurements for beads presumably driven by one and two dyneins, respectively (as determined by the observed stall force), are shown in Figures 3A and 3B. For the single-motor case (stall force of approximately 1 pN; see inset in Figure 3A), a run of approximately 1.5 μm is observed before the motor detaches, and the video track is lost because the bead diffuses away. For the case of two motors active on the bead (stall force of approximately 2 pN; inset in Figure 3B), beads often moved over long distances, as shown in Figure 3B. Ninety percent of

Table 1. Motion Properties Obtained from the Parsing of Video Tracks of Beads Driven by Single-Dynein, -Kinesin-1, and Multiple-Dynein Motors

	Single Dynein	Single Kinesin-1	Multiple Dyneins
Number of beads studied	87	81	164
Total time of motion (s)	520	202.5	2479
Total (−) motion recorded (nm)	−132366	−535	−858608
Total (+) motion recorded (nm)	+21287	+147218	+16871
Net distance moved (nm)	−111079	+146683	−841737
Net velocity (nm/s)	−213	+724	−340
Spread (SD) in velocity (nm/s)	400	278	356
Fraction of time moving in (+)	19 ± 2%	>99%	4 ± 1%
Fraction of net distance in (−)	81%	<1%	98%
Fraction of net distance in (+)	19%	>99%	2%
Mean (−) segment length (nm)	−450 (±19)	not determined	−697 (±15)
Mean (+) segment length (nm)	+192 (±13)	+698 (±33)	+130 (±12)
Mean (−) segment duration (s)	1.45 (±0.08)	not determined	1.92 (±0.04)
Mean (+) segment duration (s)	0.88 (±0.06)	0.95 (±0.04)	0.85 (±0.06)
Mean (−) velocity (nm/s)	−312 (±31)	not determined	−362 (±21)
Mean (+) velocity (nm/s)	+219 (±21)	+711 (±48)	+152 (±15)

For the single-dynein and single-kinesin statistics, only a subset of beads representing longer runs was analyzed. This was done so that end effects (termination of segment because of the run ending) could be avoided. Beads moved on straight microtubules immobilized on the coverslip surface. The motion is under conditions of no externally applied load (no optical trap). The "forward" direction of motion is toward the minus end of the microtubule for dynein and toward the plus end for kinesin-1. For kinesin-1, the amount of reverse (minus-directed) motion was too small to be quantified reliably. The minus-end segment lengths and durations for single dynein are presented for the sake of comparison with multiple-dynein motion. These values are not representative of a large population of single-dynein runs that were shorter than the reported segment length (−450 nm, minus sign implying motion directed toward the MT minus end). See also Figure 2.

the beads in the two-motor case (total of 20 tested) moved for a distance of >4 μm. Such beads usually reached the end of the MT before detaching. Thus, 4 μm is an underestimate of the run length of two-motor-driven beads. A further increase in motor concentration also led to very long runs (at least 4 μm), usually ending only when the bead reached a MT end. In both the two-motor and the three-motor case, we observed runs that were up to 8 μm in length on particularly long MTs in our experiments. As pointed out earlier, a single dynein would have less than a 1% chance of moving a bead more than 3.5 μm (see Figure 1 inset). Thus, under identical conditions in our in vitro experiment, the addition of a second motor dramatically enhanced the run length of dynein-driven beads.

Multiple Dyneins Work Together: Stall Forces Are Additive

In a continuation of the trend of higher stall forces from increased motor concentration (Figures 3A and 3B), we observed beads escaping from the optical trap with forces exceeding a value expected from three motors (see Figure 3C). These observations show that it is possible for up to four dynein motors to come together and drive motion of cargo measuring approximately 0.5 μm, which is a typical size for some cargos in vivo [22, 25]. Under our in vitro conditions, there was no requirement for additional factors (e.g., dynactin) to assemble and coordinate dynein motors on the cargo. There is limited data available on in vivo stall force of motors [13, 14], but the forces appear to be quite large. For example, in the developing *Drosophila* embryo, retrograde-moving lipid droplets driven by cytoplasmic dynein show stall forces of more than 5 pN [14], which cannot be generated by a single dynein motor. Our in vitro experiments therefore show that in the limit of multiple dynein motors driving motion, forces characteristic of in vivo dynein-based function (4 pN or more) can be achieved.

For multiple motors to generate efficient motion in vivo, we expect the motors to cooperate and thus avoid an energy-inefficient tug-of-war. To investigate if this occurs without additional cofactors, we made stall-force measurements over a range of dynein:bead concentrations and generated a histogram of stall forces (Figure 4A). Three distinct peaks with a multiplicity of approximately 1 pN can be seen. The histogram could be fitted to a sum of 3 Gaussians, whose central positions were not constrained to be multiples of each other. Because the single-dynein stall force is approximately 1 pN [5], a multiplicity of 1 pN suggests that total force is the sum of individual motor forces, and it provides evidence that motors can cooperate to generate force together. The width of stall-force distribution broadens as the motor number increases, which can be explained by the inherent variance in the stall force of a population of single motors [5]. A random choice of two or more motors drawn from this population would naturally lead to an increase in variance of the stall force and a broadening of the distribution:

$$\sigma_n = \sigma\sqrt{n}$$

(σ_n = SD of n-motor stall distribution; σ = SD of single-motor stall distribution)

The observed broadening of stall force is thus expected statistically and need not imply that the motors become uncoordinated as far as force generation is concerned. The values of multiple motor stall force and their distributions (see Figure 4A) are not statistically different (95% confidence, Student's t test) from what would be expected from a simple addition of single-motor forces.

Multiple Motors Improve Motion: The Suppression of Unproductive Backward Travels

The additive nature of dynein stall forces suggests that multiple dyneins can cooperate. Does cooperation influence the general characteristics of dynein-driven

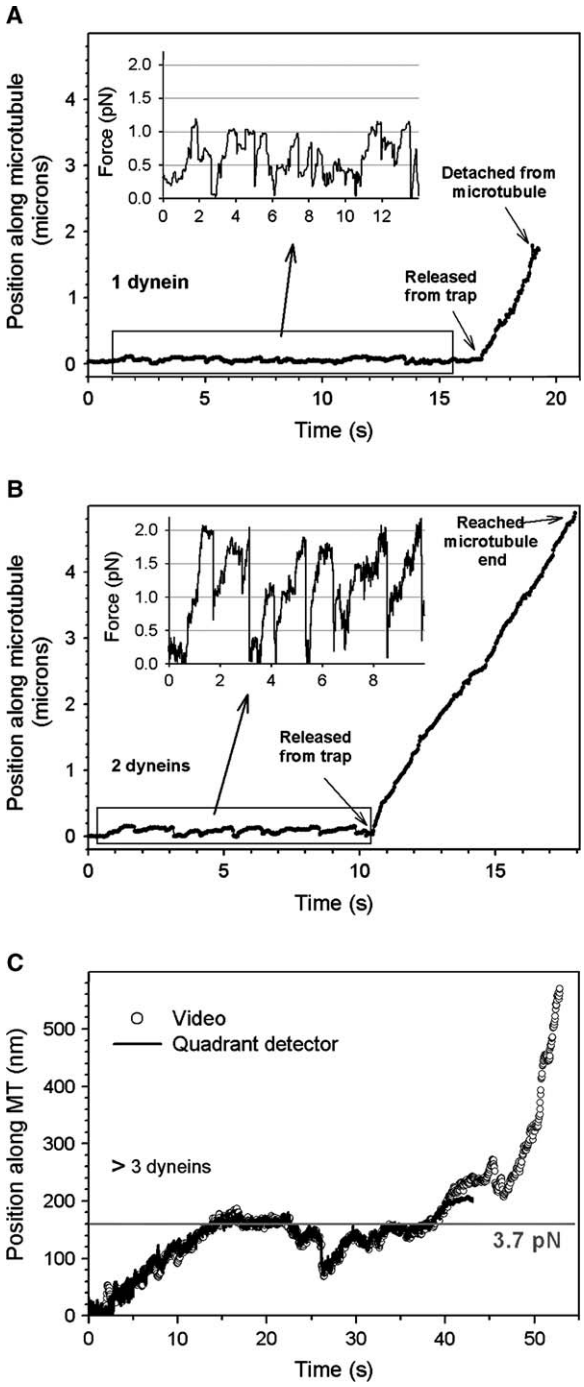

Figure 3. Multiple Dyneins Move Cargo Much Farther than a Single Dynein and Exert Higher Force

(A) Video track of (stalls + free motion) of a dynein-coated bead. A dynein-coated bead captured by the optical trap was brought onto a microtubule. The trap stiffness was 0.011 pN/nm, and ATP concentration was 3 mM. The motor generated a maximum force of approximately 1 pN (as expected for single dynein) in the trap (see inset) before it was released from the trap. The bead then moved for about 1.5 μm before detaching. A linear fit over the period of free motion yields a velocity of 509 ± 9 nm/s.

(B) Similar recording for a presumably two-dynein-driven bead. Trap stiffness is 0.013 pN/nm. Once released from the trap, the bead moves for over 4 μm before it reaches the microtubule end and stops. Note that single-dynein-driven beads have less than a 1% chance of moving more than 3.5 μm (see Figure 1A inset). A linear fit over the period of free motion yields a velocity of 601 ± 3 nm/s.

(C) Example of motion presumably driven by >3 motors. Data from the quadrant detector and video tracking have been superimposed and show close agreement. The quadrant detector is sensitive only out to approximately 160 nm from the center of the trap, and thus the two data sets match up to this limit. The trap is estimated to be linear up to approximately 160 nm, with a stiffness of 0.023 pN/nm. A weak residual force is still exerted by the trap for approximately 60 nm beyond this distance; the bead moves slowly up to approximately 220 nm, where it appears to stall briefly (see video track). Beyond 220 nm from the center of the trap, the load from the trap drops because the velocity increases and the bead moves away rapidly (see the video data > 45 s).

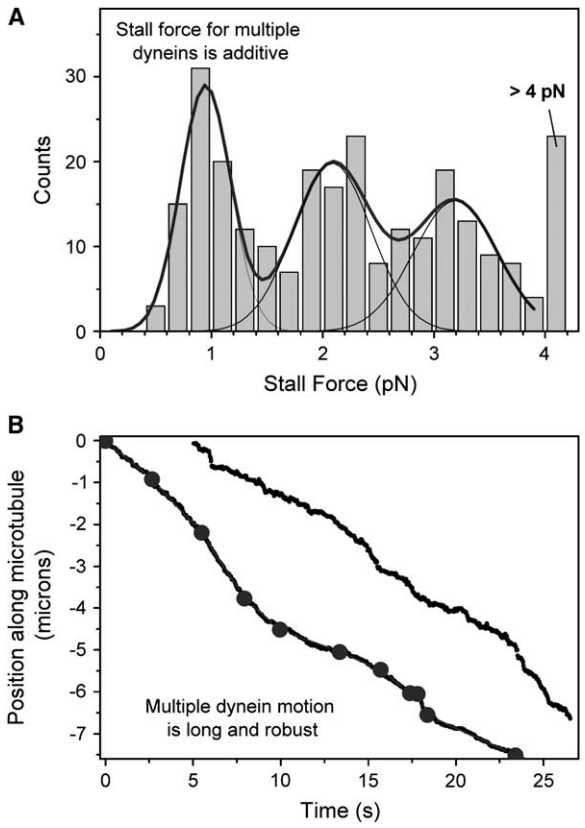

Figure 4. Global Properties of Motion Improve and Tend toward In Vivo Characteristics upon Addition of Motors

(A) Histogram of stall force measured for dynein across a range of dynein concentrations. The stall-force histogram shows a multiplicity of approximately 1 pN, which is the single-motor stall force (first peak). The peaks presumably correspond to one, two, and three motors actively generating force. All stalls exceeding 4 pN are grouped into a single bin and presumably correspond to more than three motors driving motion. A least-square fit (thick line) to the sum of three Gaussians is shown (χ^2 = 12.17, df = 9, p = 0.2). The position and spread of all peaks were free parameters during the fit. The peak values obtained from the fit are 0.94 ± 0.03 pN, 2.09 ± 0.08 pN, and 3.19 ± 0.11 pN. These values presumably correspond to one-, two-, and three-motor stall forces. The spreads (SD) of peaks from the fit are 0.23 ± 0.03 pN, 0.35 ± 0.09 pN, and 0.37 ± 0.11 pN.

(B) Video tracks of two multiple-dynein-driven beads. Both of these beads show very long runs and reach the end of the microtubule before stopping. One track shows constant-velocity segments (thick lines connected by closed circles) generated from the parsing program.

motion? Because single dynein appears to be a poor transporter, frequently entering into unproductive backward motion or pausing, there is the exciting possibility that the combination of motors suppresses the occurrence of these unproductive periods. Such suppression would help us understand how robust in vivo dynein motion is achieved. In vivo, it is not possible to determine whether the improvement in transport comes about through the use of multiple dyneins or from the multitude of accessory proteins [26] present on the cargo. Because our controlled in vitro assays utilize only purified dynein motors, we can assess whether motion is improved just by the use of multiple dyneins and, if so, to what extent.

We observed that, compared to those of single dynein, multiple-dynein motion runs were longer and usually were at higher velocities. We used the parsing program to quantify this difference. To maintain consistency, we used program control parameters that were exactly the same as those for the motion of single-dynein and kinesin motors. The segmentation of one multiple-motor-driven track is shown in Figure 4B. Note that, on average, the segments are longer than those for single-dynein motion (compare with segments in Figure 1A; see also Table 1). Histograms of velocities and segment lengths for multiple-dynein-driven motion were obtained through parsing (Figures 2E and 2F; Table 1). The frequency of backward motion for the multiple-dynein case was suppressed significantly in comparison to the single-dynein case (compare Figure 2E with Figure 2A; Figure 2F with 2B). Only 2% of the net distance moved is in the reverse direction for multiple dyneins; this is and improvement of almost an order of magnitude from the single-dynein case (Table 1). The net velocity (considering both − and + motion) of a bead driven by multiple dyneins is −340 nm/s, which is a significant improvement from the single-motor case (see Table 1). The spread in segment velocity is also smaller than for single motors (Table 1), as might be expected from the reduction in plus-directed velocity segments. It is interesting to note that the mean velocity of forward (minus directed) segments during multiple motor motion is −362 ± 21 nm/s, which is not statistically different from the velocity of −312 ± 31 nm/s in the single-dynein case ($p = 0.19$). When taken together with the large reduction in reverse segments, this shows that the improvement in motion occurs primarily through suppression of reverse-directed segments and not through some fundamental change in the mechanochemical cycle of single motors.

At room temperature, we find a minus-directed mean velocity of −362 ± 21 nm/s for multiple-motor dynein motion. This is lower than the value some other reports find for in vivo dynein-driven motion [9, 10], but it is reasonable given the reported value of −359 ± 50 nm/s for multiple-motor dynein-driven lipid-droplet motion in *Drosophila* embryos at the same temperature [22]. Some of the beads in our experiments were observed to move at sustained velocities of up to 700 nm/s, and examining these separately, we found no indication of higher stalling forces. Thus, we do not believe that the runs with the slower mean velocity reflected impaired dynein function but that they instead reflected random variation in motor function.

Comparing multiple- and single-dynein-driven motion, in addition to the change in frequency of the plus-end segments, we found a statistically significant decrease in the length of plus-end segments for multiple dyneins. This results from a decrease in mean velocity; the temporal duration of plus-end segments was unchanged (Table 1). Below, we suggest that such a velocity reduction is consistent with the unproductive period resulting from a diffusive state. The lower diffusive velocity for multiple motors (as compared to single motors) presumably implies increased drag on the diffusing bead from multiple weak attachments to the microtubule.

Because the unproductive periods of motion could significantly impair performance under load, we also investigated how motion under load changed in single- versus multiple-dynein motors. Using the same criterion as that for single dynein and kinesin-1 (see section 2 in the Supplemental Data), we scored events of backward slippage in multiple dynein-driven stall-force records. We found a significant decrease in backward slippage upon the addition of motors (Figure 1C inset), which is also clear from a visual comparison of the single-dynein stall (Figure 1C) with the multiple-dynein stalls (Figures 5A and 5C). Because individual motors share load (Figure 4A) and the comparisons were done at the same average load per motor, it appears that the presence of a second motor significantly improves the performance of the first motor under load (and vice-versa).

Steps during Multiple-Motor Motion

Because stall forces are additive (Figure 4A), we could extract segments of motion from optical-trap records where force predicts the number of active motors. For example, if the bead stalled at approximately 2 pN, it presumably had two motors driving motion. Because a single motor stalls approximately 1 pN, both motors would be actively generating force in the load regime of 1−2 pN, and hence this regime could be used to investigate the stepping behavior of two simultaneously active motors. In our experiments this interval of load corresponds to approximately 50 nm of motion in the optical trap and is thus large enough to allow detection of several successive steps. A similar strategy was also applied to motion driven by three motors. We previously reported [5] that dynein functions as a gear and can take steps of varying sizes (32, 24, 16, 8 nm) in response to an applied load. The load above which single dynein motors shift into 8 nm steps was identified as approximately 0.8 pN. Figure 5A shows the stepping behavior of a bead presumed to be two-motor driven because it stalls at approximately 2.2 pN. Successive steps of 8 nm can be clearly seen when the motors are moving under load (marked with horizontal arrows). A pairwise distance function analysis [27] confirms the 8 nm periodicity of these steps (Figure 5B). Note that the 8 nm steps seen in these records appear above approximately 1.5 pN load, which is twice the load required to effect an 8 nm transition on a single motor. This could be expected if both motors were to share load equally. The observation of 8 nm steps of the bead does not necessarily mean that the mechanochemical cycles of both motors are synchronized to occur simultaneously. This apparent coordination could be load induced because under >1.1 pN load, the bead might advance only when both

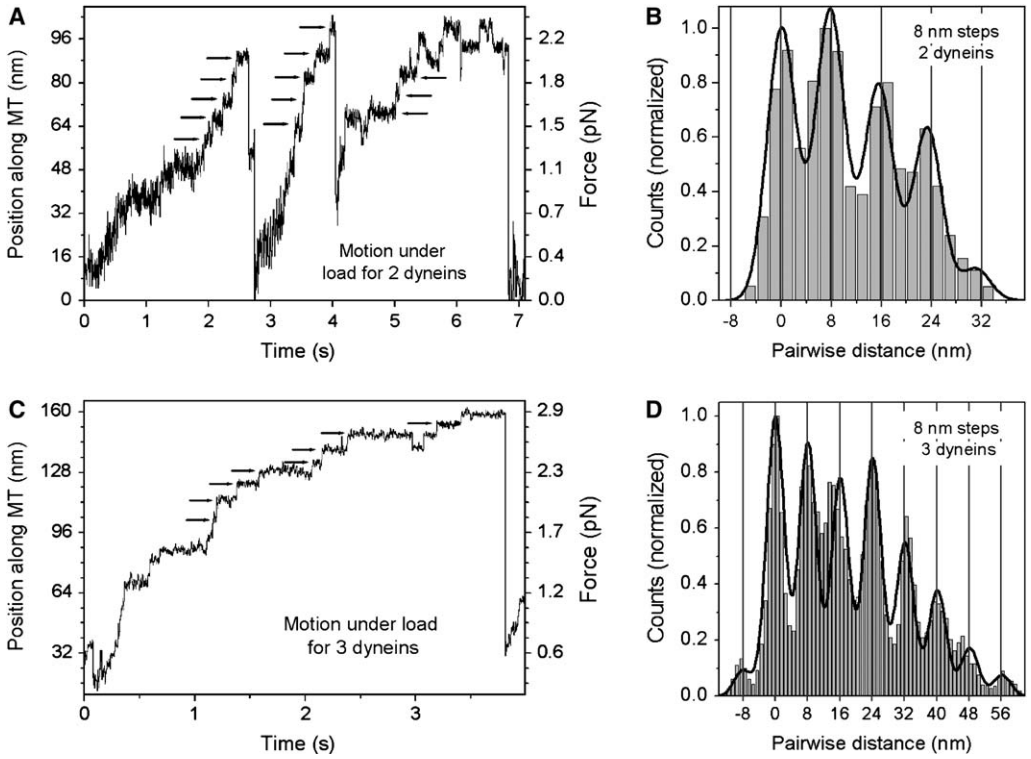

Figure 5. Beads Driven by Multiple Dyneins Show Clean 8 nm Steps under Load

(A) Stall-force record and stepping properties of motion presumably driven by two dynein motors. Horizontal arrows mark 8 nm steps. The trap stiffness was 0.023 pN.

(B) Normalized histogram of pairwise distances of the data from 2 to 2.5 s in (A). Thick dark line is a fit to sum of 5 Gaussians, which shows a periodicity of 7.8 nm ± 0.1 nm.

(C) Stall force record and steps for motion presumably driven by three dynein motors. Horizontal arrows mark 8 nm steps.

(D) Normalized histogram of pairwise distances of data from 1.3 to 3.6 s of (C). The thick dark line is a fit to sum of 8 Gaussians, step size = 8.0 nm ± 0.1 nm.

motors have completed an 8 nm step each. This situation apparently extends to three motors because we observe very clean successive 8 nm steps at loads > 2.2 pN for stalls going up to approximately 3 pN (Figures 5C and 5D).

Discussion

Nature of the Unproductive State

Our analysis shows that multiple motors improve dynein-based transport predominantly by suppressing the unproductive backward motion. Thus, it becomes important to understand why the unproductive periods arise. Two models could be imagined: (1) The motor sometimes enters an off-pathway state, where it is unproductive and under some circumstances shows backward motion or (2) The motor has a fixed probability (P_B) of taking a backward step at every pass through its hydrolytic cycle. Based on simulated data and characteristics of motion under load (see section 6 in the Supplemental Data), we can rule out the second model.

What, then, is the nature of this unproductive state? Earlier work [28] has shown that microtubules exhibit one-dimensional diffusion on a surface coated with the β-intermediate chain of a flagellar dynein. For cytoplasmic dynein, Wang et al. [21] have reported that motor bound beads show ATP-dependent diffusion on the MT surface and have suggested that the motor can exist in three different states: motile, diffusive, or inactive. We believe that the unproductive state we observe is a combination of the inactive and diffusive states suggested by Wang et al. and propose that frequent inter-conversions between the motile and unproductive states are possible. This proposal is strengthened by the observation of dynein-driven beads with a back-and-forth phase of motion preceded and succeeded by well-directed linear motion along the microtubule (see Figure 6).

To test whether the dynein bound beads diffuse, we calculated the mean squared deviation [21] of bead position along the microtubule within long back-and-forth motion segments (for example, as in Figure S5 and Figure S4C in the Supplemental Data). The averaged mean squared deviation of seven individual beads (see Figure S4D) shows a linear dependence on time, as expected for a one-dimensional random walk (diffusion along microtubule). We also analyzed such diffusing beads with our parsing program (see section 7 in the Supplemental Data) and found that the range of velocities and length of backward segments of dynein bound diffusing beads is large enough to explain the backward segments during dynein-driven motion.

The existence of a diffusive state agrees with earlier results of dynein motion on subtilisin-digested microtubules [19] and provides insight into why this unproductive state is dynein specific. Those experiments suggest that the dynein head makes two contacts with the

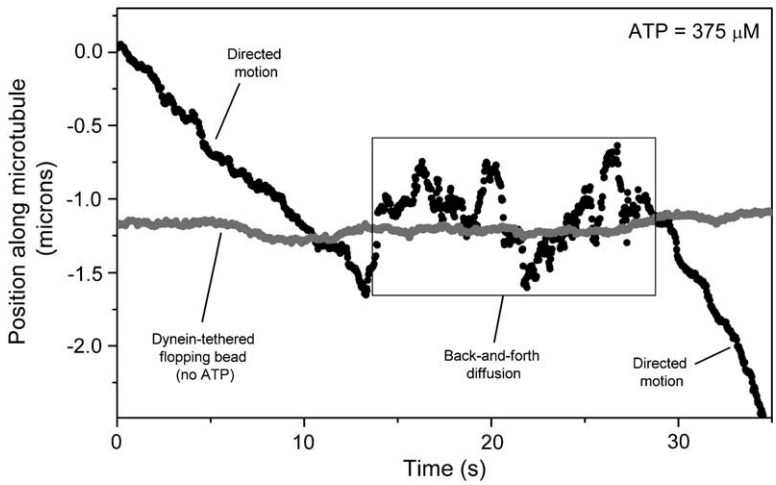

Figure 6. Dynein Interconverts between Directed-Motion and Diffusive States

(A) Back-and-forth motion along the microtubule in between two directed periods of motion. The video track of a dynein bound flopping bead in the absence of ATP (gray) is also shown for the sake of comparison (mean position adjusted for clarity). It is clear that the back-and-forth motion cannot be explained by thermal flop of the bead (see text for details).

microtubule: a first strong binding presumably mediating the power stroke and a second weak binding to the C-terminal region of the MT. The latter binding appears to be retained in axonemal dynein throughout the catalytic cycle [20], as also evidenced by processive motion of a single-headed axonemal dynein [6]. The normal dynein mechanochemical cycle presumably follows a coordinated sequence of binding and unbinding of the strong contact to achieve directed motion via a power stroke at every cycle, whereas the weak contact is retained over longer time scales. One mode of passage into the unproductive state could be that there is some chance for the strong binding to fail at every step. Once this happens, the motor is still bound to the MT via the weak binding—but then it either remains paused or can diffuse along the MT. This off-pathway state can continue for timescales larger than the average turnover time of the motor (for example, approximately 10 s; see Figure 6). Once the strong binding re-engages, the motor can re-enter the normal state and continue directed motion (Figure 6).

Because segments of diffusion can arise within directed motion (Figure 6), diffusion is not a signature from a second population of unhealthy dynein motors. Wang et al. had previously classified diffusive and unidirectionally moving beads as two distinct populations [21]. Thus, although our identification of diffusive dynein-driven motion agrees with Wang et al., our interpretation of this diffusive state and its implications are different. We believe that the unproductive paused/diffusive state is characteristic for single dynein motors and is suppressed in the presence of additional motors because the chance that strong binding of all the active motors will fail together is lower. In support of the possibility that the plus-end motions reflect diffusion, we note that in the multiple-motor case, the velocity of motion in the plus-end direction is statistically lower than that of single motors (Table 1), as might be expected due to drag from two independent diffusing attachment points. In vivo, due to the higher effective viscosity, we would expect that such periods of the diffusive state would be manifested simply as pauses, and indeed pauses are often observed in dynein-driven motion [22]. This observation suggests that at least some pauses of cargos in vivo could be due to paused dynein rather than to blocked transport resulting from steric hindrance.

Dynein Function In Vivo: The More the Better?

This ability to cooperate presumably allows multiple motors to function in vivo; otherwise, multiple-motor motion would be extremely inefficient. This cooperation does not appear to require any non-motor accessory factor. Hence, it will be interesting to understand what role the many dynein accessory proteins [26] play in vivo in achieving or regulating dynein function. The present work emphasizes that the collective behavior of a few motors could be quite different from single-molecule function. Here we focused on the improvement in function observed when we went from single-motor transport to that driven by two or three motors. The multiple dyneins spent approximately 4% of their time moving in the wrong direction, in comparison to a single kinesin-1 spending less than 1% of its time doing so. If one assumes that this 4% reflects being in the diffusive off-pathway state, and given that the diffusion distribution is symmetric around the origin, this means that there is another 4% of diffusive minus-end-directed motion that we failed to detect (i.e., a total of 8%). Based on the fraction of beads escaping from the trap, we estimate that 90% of the multiple-motor motion in our experiments was driven by two or three dyneins. So, the above-stated 8% of total diffusive motion is characteristic for two or three dyneins.

In considering in vivo function, it is interesting that during MT-based motion in the developing *Drosophila* embryo, after moving in the minus-end direction, lipid droplets spent 9% of the time in a paused state [14]. As argued above, in vivo the diffusive state probably manifests as pauses due to higher viscosity. Total in vivo pauses likely include additional effects such as competition with kinesin, obstacles in the crowded in vivo environment, and regulation of motor activity. Although we expect that the total pausing due to this off-pathway state is reduced when more motors are used, the 8% diffusion in vitro for the two- to three-motor case suggests that this mechanism could be an important contributor to the overall 9% pausing observed in vivo.

Our results indicate that up to some point, adding dynein motors improves motion—indeed, motion under load (compare backward motion in Figures 5A and 5C) shows some improvement in going from two to three motors. Perhaps this is why, in the few instances measured in vivo [13, 14], cargos use 4–6 dyneins. In fish [29] and *Xenopus* [30] melanophore cells, switching between dynein- and myosin-V-driven motion is suggested to be important for handover between microtubule-based and actin-based motion. Because myosin-V can generate a force of 3 ± 0.3 pN [31], more than three dyneins should be required to win against myosin-V during such handover.

Conclusion

Because the reported processivity of single dynein-dynactin pairs in vitro (approximately 1.5 μm) is insufficient to account for observed cargo travels in vivo, we investigated the possible contribution of additional dynein motors to improve transport. We found that that single dyneins are inefficient transporters because they frequently engage in unproductive pauses and back-and-forth motion and slip when under load. This unproductive motion likely reflects an off-pathway paused/diffusive state where dynein presumably remains attached to the MT only through a weak contact. This behavior is characteristic of dynein; kinesin-1 shows robust directed motion with rare backward segments. However, the ensemble function of multiple dynein motors leads to very long travels of more than 4 μm and also suppresses the unproductive off-pathway state. With multiple dyneins we observe long run-lengths, high velocities, and stall forces reminiscent of in vivo dynein function. There appears to be no requirement for additional cofactors (e.g., dynactin) to effect this improvement, but dynactin does play important additional roles in dynein regulation and could additionally improve transport that involves multiple dyneins. We earlier hypothesized [32] that the complexity of dynein architecture makes it a less robust motor. Here we show that this robustness could be regulated through the use of additional dynein motors in vitro, although it remains to be seen what implications such regulation of robustness has in the context of in vivo motion. Using the control possible with in vitro motility assays, we show that addition of single motors gives rise to certain characteristics of in vivo motion. Through this work, we hope to introduce controlled in vitro experiments on increasingly complex motor assemblies as an alternative route to understanding in vivo molecular motor function.

Experimental Procedures

Protein Purification

Twice-cycled bovine brain tubulin was purified over a phosphocellulose column [33], frozen dropwise in liquid nitrogen, and stored at −80ºC. Kinesin-1 and cytoplasmic dynein were purified from bovine brain tissue via a nucleotide-dependent microtubule-affinity procedure essentially as described [34] except that the binding step utilized both 1 mM AMP-PNP and ATP depletion by the addition of 1 unit hexokinase and 10 mg glucose per ml of high-speed brain supernatant. The dynein and kinesin-1 were further purified from each other and from dynactin with sucrose gradient centrifugation and subsequent anion exchange chromatography. No kinesin or dynactin was present in the dynein samples, and no dynein or dynactin was present in the kinesin-1 samples as determined by SDS-PAGE and Western blotting. The dynein was stored at 4ºC and used within three days of purification. The kinesin-1 was diluted into 45% glycerol and stored at −20ºC.

In Vitro Motility Assay

In vitro motility assays were performed as reported earlier [5]. All experiments were done at 24ºC in a flow chamber (volume of approximately 10 μl) made with clean poly-L-lysine-coated coverslips stuck to a microscope slide. Taxol-stabilized microtubules were flowed in so they were parallel to each other and horizontal in the microscope field of view. Microtubules were incubated to immobilize them on the coverslip surface; then the coverslip was blocked with casein (5 mg/ml). Purified dynein at required concentrations was first incubated with carboxylated polystyrene beads (490 nm diameter, Polysciences Inc.) in assay buffer (AB = ATP + 0.3 × PMEE′ + 1 mM GTP + 20 μM Taxol). PMEE′ = 35 mM PIPES (pH 7.2), 5 mM $MgSO_4$, 1 mM EGTA, and 0.5 mM EDTA. For controlling the number of dynein motors per bead, the amount of dynein in the incubation mixture was varied. Binding of dynein to beads was blocked after 5 min by the addition of casein (5 mg/ml in AB) to the incubation mixture. For kinesin-related experiments, a similar procedure and geometry was used with minor modifications. Dynein- or kinesin-coated beads were viewed with video-enhanced differential-interest-contrast (DIC) microscopy in an inverted microscope (modified Nikon TE-200). Custom-built image-processing software developed in Labview 6.1 (National Instruments) was used for video tracking. The standard deviation in the position of a fixed bead was found to be approximately 3 nm. Verification of sub-pixel resolution and details of performance of the video-tracking routine have been reported elsewhere [35]. Further details regarding the estimation of the number of motors on beads in the single-motor and multiple-motor limit can be found in section 5 of the Supplemental Data.

Optical Trapping

Optical trapping was performed with either an 830 nm single-mode diode laser with beam circularization optics (Melles Griot, CA) or a 980 nm single-mode diode laser (Axcel Photonics, MA). Trap stiffness was calculated from the power spectrum of thermal oscillations of a trapped bead and also by the viscous drag method [36]. The laser power was varied to obtain desired trap stiffness in the range of 0.01–0.05 pN/nm. Back-focal-plane imaging of bead position in the optical trap was done with a quadrant photo-diode detector. For calibration of the quadrant detector, a fixed bead was moved in known increments across the trap position with a piezoelectric stage. The detector output signal was anti-alias filtered at 1 KHz and digitized at 2 KHz. Data-acquisition and -analysis software was developed in Labview 6.1 (National Instruments). The correction factor to bead displacement due to elasticity of the bead-dynein linkage was determined to be quite small (approximately 1.06), as reported earlier [5].

Supplemental Data

Supplemental Data are available with this article online at http://www.current-biology.com/cgi/content/full/15/23/2075/DC1/.

Acknowledgments

This work was supported by National Institutes of Health grants 1RO1GM070676 to S.P.G. and NS48501 to S.J.K. The theoretical work was also supported by National Institute of General Medical Sciences grant GM-64624-01 to S.P.G. with a supplement for the Study of Complex Biological Systems. R.M. acknowledges a long-term fellowship from the Human Frontier Sciences Program. The authors acknowledge C. Yu and G. Shubeita for useful discussions. B.C. Carter and S. Cermelli are thanked for help with experiments. Thanks to P. Fordyce of the Block lab for generously sharing a carbodiimide binding protocol.

Received: September 16, 2005
Revised: October 12, 2005
Accepted: October 14, 2005
Published: December 5, 2005

References

1. Vale, R.D., and Milligan, R.A. (2000). The way things move: Looking under the hood of molecular motor proteins. Science *288*, 88–95.
2. Hirokawa, N., and Takemura, R. (2004). Molecular motors in neuronal development, intracellular transport and diseases. Curr. Opin. Neurobiol. *14*, 564–573.
3. Visscher, K., Schnitzer, M.J., and Block, S.M. (1999). Single kinesin molecules studied with a molecular force clamp. Nature *400*, 184–189.
4. Svoboda, K., and Block, S.M. (1994). Force and velocity measured for single kinesin molecules. Cell *77*, 773–784.
5. Mallik, R., Carter, B.C., Lex, S.A., King, S.J., and Gross, S.P. (2004). Cytoplasmic dynein functions as a gear in response to load. Nature *427*, 649–652.
6. Sakakibara, H., Kojima, H., Sakai, Y., Katayama, E., and Oiwa, K. (1999). Inner-arm dynein c of Chlamydomonas flagella is a single-headed processive motor. Nature *400*, 586–590.
7. Singh, M.P., Mallik, R., Gross, S.P., and Yu, C.C. (2005). Monte Carlo modeling of single-molecule cytoplasmic dynein. Proc. Natl. Acad. Sci. USA *102*, 12059–12064.
8. Fisher, M.E., and Kolomeisky, A.B. (2001). Simple mechanochemistry describes the dynamics of kinesin molecules. Proc. Natl. Acad. Sci. USA *98*, 7748–7753.
9. Presley, J.F., Cole, N.B., Schroer, T.A., Hirschberg, K., Zaal, K.J., and Lippincott-Schwartz, J. (1997). ER-to-Golgi transport visualized in living cells. Nature *389*, 81–85.
10. Ma, S., and Chisholm, R.L. (2002). Cytoplasmic dynein-associated structures move bidirectionally in vivo. J. Cell Sci. *115*, 1453–1460.
11. King, S.J., and Schroer, T.A. (2000). Dynactin increases the processivity of the cytoplasmic dynein motor. Nat. Cell Biol. *2*, 20–24.
12. Wang, Z., Khan, S., and Sheetz, M.P. (1995). Single cytoplasmic dynein molecule movements: characterization and comparison with kinesin. Biophys. J. *69*, 2011–2023.
13. Ashkin, A., Schutze, K., Dziedzic, J.M., Euteneuer, U., and Schliwa, M. (1990). Force generation of organelle transport measured in vivo by an infrared laser trap. Nature *348*, 346–348.
14. Gross, S.P., Welte, M.A., Block, S.M., and Wieschaus, E.F. (2000). Dynein-mediated cargo transport in vivo. A switch controls travel distance. J. Cell Biol. *148*, 945–956.
15. Habermann, A., Schroer, T.A., Griffiths, G., and Burkhardt, J.K. (2001). Immunolocalization of cytoplasmic dynein and dynactin subunits in cultured macrophages: Enrichment on early endocytic organelles. J. Cell Sci. *114*, 229–240.
16. Welte, M.A. (2004). Bidirectional transport along microtubules. Curr. Biol. *14*, R525–R537.
17. Gross, S.P. (2004). Hither and yon: A review of bi-directional microtubule-based transport. Physical Biology *1*, R1–R11.
18. Thorn, K.S., Ubersax, J.A., and Vale, R.D. (2000). Engineering the processive run length of the kinesin motor. J. Cell Biol. *151*, 1093–1100.
19. Wang, Z., and Sheetz, M.P. (2000). The C-terminus of tubulin increases cytoplasmic dynein and kinesin processivity. Biophys. J. *78*, 1955–1964.
20. Koonce, M.P., and Tikhonenko, I. (2000). Functional elements within the dynein microtubule-binding domain. Mol. Biol. Cell *11*, 523–529.
21. Wang, Z., and Sheetz, M.P. (1999). One-dimensional diffusion on microtubules of particles coated with cytoplasmic dynein and immunoglobulins. Cell Struct. Funct. *24*, 373–383.
22. Welte, M.A., Gross, S.P., Postner, M., Block, S.M., and Wieschaus, E.F. (1998). Developmental regulation of vesicle transport in Drosophila embryos: Forces and kinetics. Cell *92*, 547–557.
23. Hill, D.B., Plaza, M.J., Bonin, K., and Holzwarth, G. (2004). Fast vesicle transport in PC12 neurites: Velocities and forces. Eur. Biophys. J. *33*, 623–632.
24. Rief, M., Rock, R.S., Mehta, A.D., Mooseker, M.S., Cheney, R.E., and Spudich, J.A. (2000). Myosin-V stepping kinetics: a molecular model for processivity. Proc. Natl. Acad. Sci. USA *97*, 9482–9486.
25. Rogers, S.L., Tint, I.S., Fanapour, P.C., and Gelfand, V.I. (1997). Regulated bidirectional motility of melanophore pigment granules along microtubules in vitro. Proc. Natl. Acad. Sci. USA *94*, 3720–3725.
26. Vallee, R.B., Williams, J.C., Varma, D., and Barnhart, L.E. (2004). Dynein: An ancient motor protein involved in multiple modes of transport. J. Neurobiol. *58*, 189–200.
27. Svoboda, K., Schmidt, C.F., Schnapp, B.J., and Block, S.M. (1993). Direct observation of kinesin stepping by optical trapping interferometry. Nature *365*, 721–727.
28. Vale, R.D., Soll, D.R., and Gibbons, I.R. (1989). One-dimensional diffusion of microtubules bound to flagellar dynein. Cell *59*, 915–925.
29. Rodionov, V., Yi, J., Kashina, A., Oladipo, A., and Gross, S.P. (2003). Switching between microtubule- and actin-based transport systems in melanophores is controlled by cAMP levels. Curr. Biol. *13*, 1837–1847.
30. Gross, S.P., Tuma, M.C., Deacon, S.W., Serpinskaya, A.S., Reilein, A.R., and Gelfand, V.I. (2002). Interactions and regulation of molecular motors in Xenopus melanophores. J. Cell Biol. *156*, 855–865.
31. Mehta, A.D., Rock, R.S., Rief, M., Spudich, J.A., Mooseker, M.S., and Cheney, R.E. (1999). Myosin-V is a processive actin-based motor. Nature *400*, 590–593.
32. Mallik, R., and Gross, S.P. (2004). Molecular motors: Strategies to get along. Curr. Biol. *14*, R971–R982.
33. Sloboda, R.D., and Rosenbaum, J.L. (1982). Purification and assay of microtubule-associated proteins (MAPs). Methods Enzymol. *85* (Pt. B), 409–416.
34. Schroer, T.A., and Sheetz, M.P. (1991). Two activators of microtubule-based vesicle transport. J. Cell Biol. *115*, 1309–1318.
35. Carter, B.C., Shubeita, T.G., and Gross, S.P. (2005). Tracking single particles: A user-friendly quantitative evaluation. Physical Biology *2*, 60–72.
36. Rice, S.E., and Spudich, J.A. (2003). Building and using optical traps to study properties of molecular motors. Methods Enzymol. *361*, 112–133.